RESEARCH PAPER

PCCP
www.rsc.org/pccp

Mn oxidation states in tri- and tetra-nuclear Mn compounds structurally relevant to photosystem II: Mn K-edge X-ray absorption and Kβ X-ray emission spectroscopy studies

Shelly A. Pizarro,†[ab] Pieter Glatzel,[c] Hendrik Visser,‡[ab] John H. Robblee,§[ab] George Christou,[d] Uwe Bergmann*[e] and Vittal K. Yachandra*[a]

[a] *Melvin Calvin Laboratory, Physical Biosciences Division, Lawrence Berkeley National Laboratory, Berkeley, CA 94720. E-mail: VKYachandra@lbl.gov; Fax: +1 (510) 486-6059; Tel: +1 (510) 486-4330*

[b] *Department of Chemistry, University of California, Berkeley, CA 94720, USA*

[c] *Department of Inorganic Chemistry and Catalysis, Utrecht University, 3584 CA Utrecht The Netherlands*

[d] *Department of Chemistry, University of Florida, Gainesville, FL 32611, USA*

[e] *The Stanford Synchrotron Radiation Laboratory, 2575 Sand Hill Rd, Menlo Park, CA 94025, USA. E-mail: bergmann@ssrl.slac.stanford.edu; Fax: +1 (650) 926-3600; Tel: +1 (650) 926-3048*

Received 18th May 2004, Accepted 10th September 2004
First published as an Advance Article on the web 1st October 2004

X-Ray spectroscopy is used to examine the effect of the manganese oxidation state for a series of Mn model compounds. Sensitive to Mn oxidation and structural symmetry, X-ray absorption and emission spectroscopy (XAS and XES) provide complementary insights. However, few benchmark examples of complexes with similar structures but in different oxidation states are available to evaluate data from unknown structures like the oxygen evolving complex (OEC) of Photosystem II (PSII). This study examines two types of compounds prepared in a variety of Mn oxidation states and which possess chemical structures with Mn–Mn interactions (~2.7 Å and ~3.3 Å) that have been observed in the OEC. Model complexes with core compositions Mn_3O and Mn_4O_2 contain combinations of Mn in either a reduced (II) or oxidized (III) state. Within each set of compounds, complexes with higher Mn oxidation states have absorption K-edge energy values that are higher (1.6–2.2 eV) than those of their more reduced counterparts. This trend is accordingly reversed in the Kβ emission spectroscopy where the first moment energy values are lower (0.09–0.12 eV) for compounds with higher Mn oxidation states. We will discuss in detail, how these trends can be quantitatively used to characterize the effects of the Mn oxidation state as well as the surrounding ligand environment on the observed X-ray spectra. The results are discussed with respect to previously obtained data on different S-states of the OEC.

1 Introduction

X-ray spectroscopy is ideally suited to study the oxidation state of an element within a protein because the element in question can be selectively probed without interference from the surrounding matrix. A number of redox-active metal centers within metalloproteins have been well characterized using X-ray absorption near edge structure (XANES) spectroscopy [1–7] and recent innovations in detection instrumentation[8,9] have now enabled the collection of X-ray emission spectra (XES) from such biological systems.

The photosynthetic oxygen evolution center (OEC) of Photosystem II (PSII) is a Mn_4Ca cluster that undergoes a cycle of four intermediate S-states (S_0, S_1, S_2, S_3) before releasing dioxygen during the $S_3 \rightarrow S_0$ transition.[10] The precise structure and mechanism that enable this catalytic function are unknown. X-ray crystallography studies at 3.7 Å and 3.6 Å resolution have identified electron density corresponding to the metal center and have proposed a bent 'Y' shaped Mn cluster.[11,12] Most recently, Ferreira *et al.*[13] propose a cubane-like structure for the Mn_4Ca cluster but the resolution of 3.5 Å is not sufficient for a definitive conclusion. EXAFS analysis of the OEC have provided parameters that are consistent with several topological models.[14–17] Previous XAS studies show that there is a consensus of Mn–Mn interactions within the cluster with one mono-μ-oxo (~3.3 Å) and two or three di-μ-oxo (~2.7 Å) bridges.[16–18] Sr and Ca EXAFS have demonstrated the proximity of Ca(Sr) to the Mn and the presence of a Mn_4Ca cluster in the OEC.[19,20] The ultimate structure of the OEC has significant implications for the mechanism of water oxidation. Although the Kok cycle establishes a series of oxidation steps in PSII before dioxygen release, there is much debate over the role of the Mn and its oxidation state, in particular during the $S_2 \rightarrow S_3$ transition.[14–17] It is therefore important to study known model systems to provide a sound framework for discussion of unknown structures.

XANES and XES have different underlying physical processes[21] and are complementary tools to probe the Mn electronic environment. The strongest features in XANES arise from 1s → 4p electronic absorption (Fig. 1A) and are typically preceded by a small feature assigned to the dipole-'forbidden' 1s → 3d transition. Observed changes in the shape and

† Current address: Sandia National Labs, Biosystems Research Dept, P.O. Box 969, Livermore, CA 94551-0969, USA.
‡ Current address: California Institute for Quantitative Biomedical Research, University of California, Berkeley, CA 94720, USA.
§ Current address: Dept of Chemistry, Massachusetts Institute of Technology, Cambridge, MA, 02139, USA.

DOI: 10.1039/b407513g

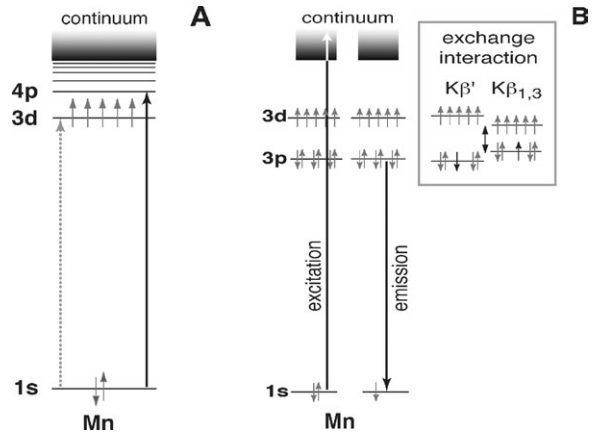

Fig. 1 Energy level diagram of the electronic excitation and emission processes involved in (A) XANES and (B) Kβ XES. The dipole-forbidden pre-edge transition in XANES is shown as a dotted gray line while the XES exchange interaction is shown alongside the emission pathway in an inset box.

position of this K-edge have been attributed to oxidation state, symmetry, ligand environment, and electronic coupling. Kβ XES is based on measuring the spectral distribution of the 3p → 1s transition (Fig. 1B) after 1s core hole excitation. The exchange interaction of the unpaired 3d electrons with the 3p hole in the final state of the 3p → 1s fluorescence transition leads to two spectral features: Kβ′ for parallel interactions and $K\beta_{1,3}$ for antiparallel interactions.[22] Because the number of unpaired 3d electrons relates directly to the oxidation state in high-spin systems, changes in the Kβ′-$K\beta_{1,3}$ splitting can be used to quantify changes in the oxidation state.[23,24] In comparison to XANES, the intrinsically different nature of the Kβ XES shifts leads to a lesser dependence on the surrounding ligand environment thus enabling a more reliable measure of oxidation state changes in the probed element. Visser *et al.*[25] have demonstrated this technique for a series of Mn-oxo binuclear complexes prepared electrochemically and reported consistent decreases in the $K\beta_{1,3}$ first moment energy for Mn(II,III → III,IV → IV,IV) oxidation state changes. PSII has also been recently characterized using Kβ XES. The Mn_4Ca cluster of the OEC was examined at each transition step of the Kok cycle; the change in the $K\beta_{1,3}$ first moment energy during the $S_2 \rightarrow S_3$ transition was deemed too small to attribute to a change in the Mn oxidation.[26] XANES data from other groups[27,28] dispute this conclusion. In the work presented here, we will scrutinize Kβ XES and XANES techniques with structural model compounds relevant to the OEC. The results can then be used as indicators of analogous changes in Mn oxidation in the OEC and other metalloproteins.

The two sets of compounds studied contain the expected structural motifs of the OEC Mn cluster (~2.7 Å and ~3.3 Å Mn–Mn interactions). The compounds with a Mn_3O core share a mono-μ-oxo bridge while the tetranuclear Mn compounds have both mono-μ-oxo and di-μ-oxo Mn–Mn moieties (Fig. 2). In each case, we examine a set of two compounds where one compound has all Mn moieties in the Mn^{III} state and its structural analog has one Mn^{II} while the other Mn atoms remain at Mn^{III}. We will show how the Mn oxidation state contributes to changes in both the XANES and Kβ XES. Within each set, the more oxidized compounds possess a higher XANES K-edge energy and conversely a lower $K\beta_{1,3}$ first moment energy relative to the Mn^{II}-containing compounds. To assess the sensitivity of each technique to the overall ligand environment, we compare the difference spectra of the XANES and Kβ XES across each set of compounds. In addition, the symmetry of the Mn_3O core is strongly affected by the presence of the Mn^{II} atom and this has important consequences in the observed spectra that are particularly evident in the XANES

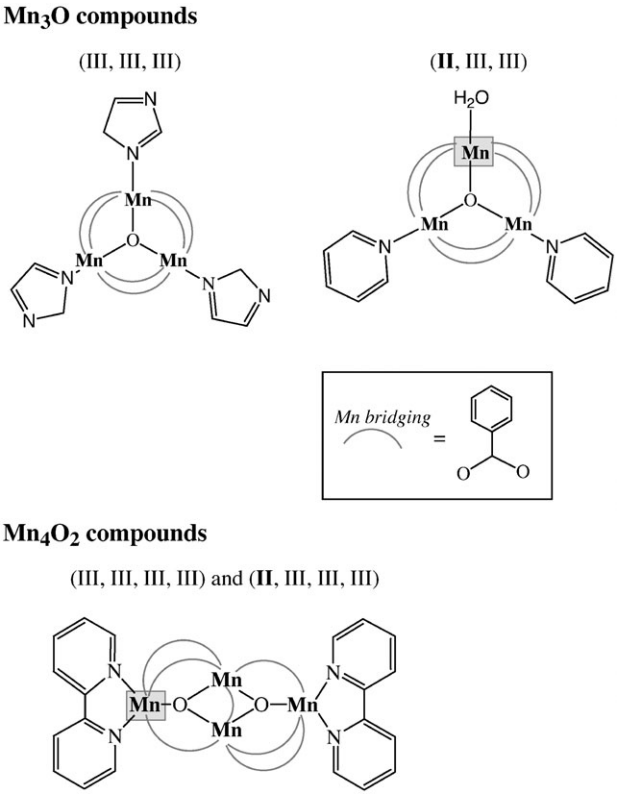

Fig. 2 Schematic of structures for the Mn model compounds. The bridging carboxylate groups are simplified as a curve for clarity in viewing the core structure and are presented in an inset box. The Mn atoms that are reduced to +2 are highlighted in grey, all other Mn atoms are in the +3 oxidation state.

and EXAFS data. Applying these methods to model systems, we will show that the combination of these two spectroscopic techniques provides a powerful tool for determining changes in the oxidation state of a redox-active metal center.

2 Experimental

2.1 Sample preparation

This study examines four model compounds possessing two different types of core structures (Mn_3O or Mn_4O_2) surrounded by different types of aromatic ligands as shown in Fig. 2. The trinuclear Mn compounds exhibit Mn oxidation states of (III,III,III) and (II,III,III)[29–31] while the tetranuclear compounds have Mn oxidation states of (III,III,III,III), and (II,III,III,III).[32–35] For convenience in the text discussion, the compounds are labeled according to core structure and the relative Mn oxidation state as follows: **Mn_3O(III)** for the oxidized trinuclear Mn species and **Mn_3O(II)** for the reduced analog; likewise **Mn_4O_2(III)** and **Mn_4O_2(II)**. Samples for XAS measurements were prepared by diluting each model compound with boron nitride in a 1 : 10 ratio then packing this powder mixture into 0.5 mm thick aluminum sample holders (4 mm × 20 mm) sealed with Mylar windows. For Kβ XES, the compounds were not diluted and were packed into slightly thicker aluminum sample holders (1 mm) sealed with Kapton windows.

2.2 X-ray absorption spectroscopy

XAS data were gathered at beam lines 2–3 and 9–3 of the Stanford Synchrotron Radiation Laboratory, operating at 3.0 GeV with beam currents between 70 and 100 mA. Details of the experimental set-up have been previously described[14,36–38] and are summarized here. A monochromator outfitted with Si ⟨220⟩ crystals detuned to 50% was used to provide radiation in

the 6.4–7.1 keV energy range. Sample temperature was maintained at 10 ± 2 K with a liquid helium cryostat (Oxford Instruments, Bedford, MA). Data were collected as fluorescence excitation spectra using either a Lytle detector filled with argon gas, or a cooled 13-element Ge detector, placed orthogonal to the incident beam. Scans were collected from 6520 to 7100 eV, with step sizes of 0.2 eV in the XANES region (6535 to 6575 eV) and 0.5 $Å^{-1}$ in the EXAFS region (k = 2 to 12 $Å^{-1}$). Energy calibration was achieved by simultaneous reference to the pre-edge XAS feature from $KMnO_4$ (6543.3 eV, FWHM ≤ 1.7 eV).

The method of data preparation for XANES and EXAFS analysis has been previously documented.[14,38] For each sample, all measured absorption scans were calibrated and then combined to improve the signal-to-noise ratio. The pre-edge background was fit to a straight line and subtracted from the spectra. The data were then divided by the Mn free-atom absorption and normalized to unity at the absorption edge by extrapolating a quadratic line fit from the post edge region (>7000 eV) to intersect with the rising edge. The K-edge energy position was deduced from the inflection point energy (IPE) of the main absorption edge as determined from the zero-crossing of its second derivative. Analytical differentiation of the absorption edge utilized a third-order polynomial fit over a region of specified length. The data were subjected to differentiation intervals of 5 eV (±2.5 eV from each data point) and 2 eV (±1.0 eV) to assess the variability in the IPE value due to the size of the differentiation interval. The 5 eV interval is typically used for PS II XAS data.

For analysis of the EXAFS region, an initial background removal was performed by fitting a quadratic or polynomial line to the post edge region and subtracting it from the spectra. As previously described,[15] the resulting spectra were then converted into a photoelectron wave vector denoted as 'k-space' and weighted by k^3. A spline function was subtracted prior to performing a Fourier transform (FT). The FT contains peaks appearing at R' representing scatterers at average distance $\langle R \rangle$ from Mn. Due to the phase shift, the apparent distance R' is generally less than $\langle R \rangle$ by 0.2–0.5 Å.

2.3 Kβ X-ray emission spectroscopy

Kβ XES measurements were performed at the SSRL beamline 10–2. A water cooled Si ⟨111⟩ double crystal monochromator was operated at 8.5 keV excitation energy and a beam size of 1 mm vertical by 5 mm horizontal. Samples were at room temperature and incident flux and sample exposure were chosen to minimize spectral changes due to radiation damage. Incident flux (I_0) was recorded with a gas filled ion chamber, and the spectra were normalized by dividing the recorded fluorescence intensity by I_0. The spectrometer used for Kβ XES experiments has been previously described in detail.[9] Briefly, the fluorescence spectrum emitted from the sample is analyzed using eight spherically curved Si ⟨440⟩ analyzer crystals operating on intersecting Rowland circles at Bragg angles close to backscattering (~84°). It captures a solid angle of 0.07 sr and has an energy resolution of ~0.7 eV. This is less than one fifth of the Kβ main line width, hence instrumental broadening is negligible. Calibration of the emission energy is obtained by assigning the first moment (using an energy interval from 6485 eV to 6495 eV) of a Mn_2O_3 (solid sample) spectrum to 6490.40 eV.[25]

3 Results

3.1 Mn XANES

Figs. 3 and 4 show the Mn K-edge XANES and its second derivative for the Mn_3O and Mn_4O_2 compounds respectively.

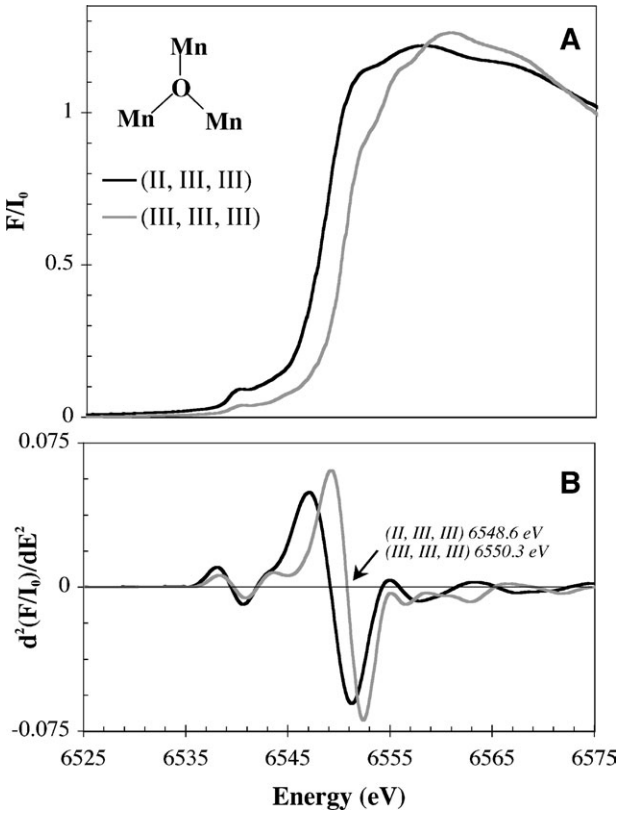

Fig. 3 (A) Mn K-edge X-ray absorption near-edge structure (XANES) and (B) its second derivative for each of the **Mn_3O** compounds. The second derivative function is taken with a 5 eV differentiation interval and the zero-crossing of the main absorption feature (as indicated by an arrow) represents the inflection point energy (IPE) for each compound.

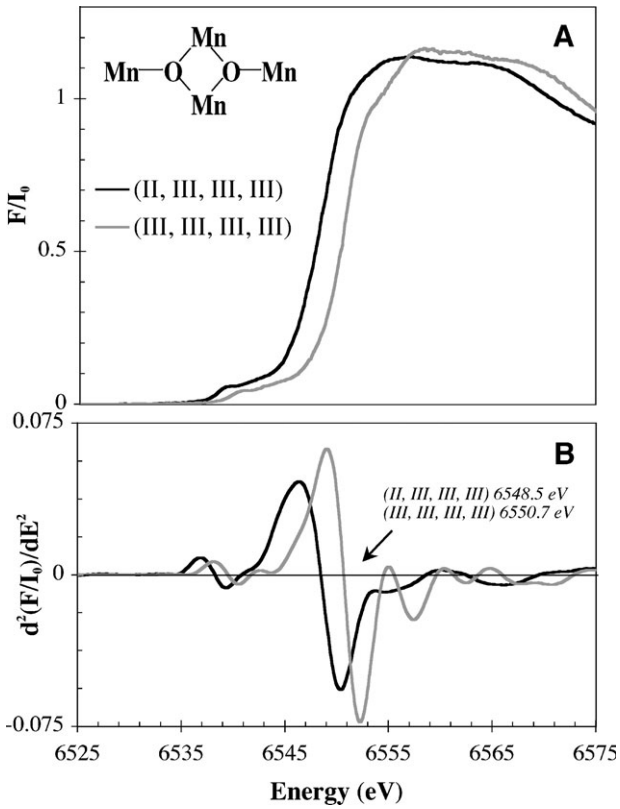

Fig. 4 (A) Mn K-edge X-ray absorption near-edge structure (XANES) and (B) its second derivative for each of the **Mn_4O_2** compounds. The second derivative function is taken with a 5 eV differentiation interval and the zero-crossing of the main absorption feature (as indicated by an arrow) represents the inflection point energy (IPE) for each compound.

Table 1 Mn K-edge absorption energy and Mn Kβ 1st moments

Model compound				
Label	Chemical formula*	Mn oxidation state	XANES Mn K-edge energy/eV	XES (Kβ) first moment energy/eV
Mn_3O(III)	$[Mn_3O(O_2Cph)_6(ImH)_3](ClO_4)_2(NBu_4)$	III,III,III	6550.27	6490.51
Mn_3O(II)	$[Mn_3O(O_2Cph)_6(py)_2(H_2O)]0.5\ CH_3CN$	II,III,III	6548.63	6490.63
			$\Delta = 1.64$ eV	$\Delta = 0.12$ eV
Mn_4O_2(III)	$[Mn_4O_2(O_2Cph)_7(bipy)_2](ClO_4)$	III,III,III,III	6550.69	6490.45
Mn_4O_2(II)	$[Mn_4O_2(O_2Cph)_7(bipy)_2]$	II,III,III,III	6548.49	6490.54
			$\Delta = 2.20$ eV	$\Delta = 0.09$ eV

The K-edge absorption energy, as the inflection point energy (IPE), is derived from the zero-crossing of the second derivative of the XANES. The differentiation interval of each derivative calculation is 5 eV; using a smaller smoothing interval (2 eV) showed only small variations in each IPE position (0.0–0.2 eV). In the XES measurement, the first moment is obtained over an energy interval from 6485 to 6495 eV. The energy was calibrated by assigning the first moment of a Mn_2O_3 reference sample to 6490.40 eV. Reproducibility between runs is within 0.01 eV. *Chemical abbreviations: bipy = bipyridine, Im = imidazole, ph = phenyl, py = pyridine.

In each case, the more oxidized compound of the set produces a XANES profile that is shifted to higher energy and has subtle changes in the overall shape. The magnitude of the shift depends on the type of compound. The inflection point energy (IPE), taken as the zero crossing of the second derivative is typically reported as the K-edge energy and these are summarized in Table 1. In the case of the Mn_3O compounds, the Mn K-edge is 1.64 eV higher for the more oxidized compound **Mn_3O(III)** than for its reduced counterpart **Mn_3O(II)**, while in the tetranuclear set, **Mn_4O_2(III)** has an IPE that is 2.20 eV higher than that of **Mn_4O_2(II)**. To compare the shape of the edge shifts in the two sets of compounds, the difference XANES spectra (*i.e.*, within a set of compounds, the XANES of the reduced compound minus that of the oxidized compound) is shown in Fig. 6A later. The absorption profile of each compound is affected to different degrees upon changing the Mn oxidation state. As in the IPE values, the Mn oxidation state appears to have a greater effect on the XANES of the Mn_4O_2 compounds thereby producing a larger negative feature at ~6550 eV. The area >6555 eV, typically indicative of ligand interactions, also reflects the differences in the overall ligand environment of the Mn atoms between the two sets of compounds despite similarities in the Mn oxidation state.

3.2 Kβ XES

The Kβ XES spectra of all four compounds are presented in Fig. 5. The weaker Kβ′ peak is at ~6476 eV while the much stronger $K\beta_{1,3}$ peak occurs at ~6492 eV. Within each set, the Mn^{II} containing compounds have a larger Kβ′ feature while the $K\beta_{1,3}$ peak is shifted slightly in position to higher energy.

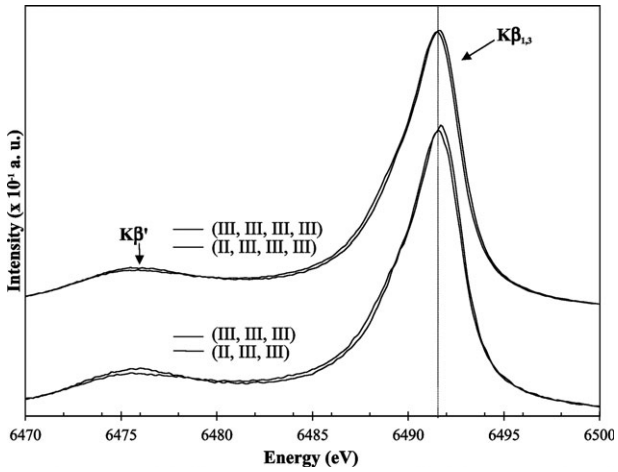

Fig. 5 Kβ X-ray emission spectra (XES) for the **Mn_3O** and **Mn_4O_2** compounds (displayed offset in magnitude for clarity).

We characterize the $K\beta_{1,3}$ energy with the first moment $\langle E \rangle$, using an energy interval from 6485 to 6495 eV. The $K\beta_{1,3}$ $\langle E \rangle$ values for each compound and the observed differences in magnitude are summarized in Table 1. Opposite in effect to XANES, the more oxidized compound within each set exhibits a lower $\langle E \rangle$ for the $K\beta_{1,3}$ peak compared to its reduced analog. It is important to note that the observed shifts in $\langle E \rangle$ scale with the fractional change in oxidation state: 0.12 eV for Mn_3O (1 out of 3) and 0.09 eV for Mn_4O_2 (1 out of 4). This indicates that $K\beta_{1,3}$ XES first moment shifts are a reliable method in measuring oxidation states. Furthermore, Fig. 6B shows that the difference Kβ XES spectra of each set of compounds have very similar shapes despite differences in core structure and terminal ligands. The position of the maximum and minimum features is unchanged in the two sets of compounds, and applying a scaling factor to compensate for the varying number of Mn atoms in each set produces nearly identical amplitudes and profiles (data not shown). This shows that, compared to XANES, Kβ XES is more susceptible to changes in oxidation state rather than differences in the overall ligand environment and is reliable in determining Mn oxidation states.

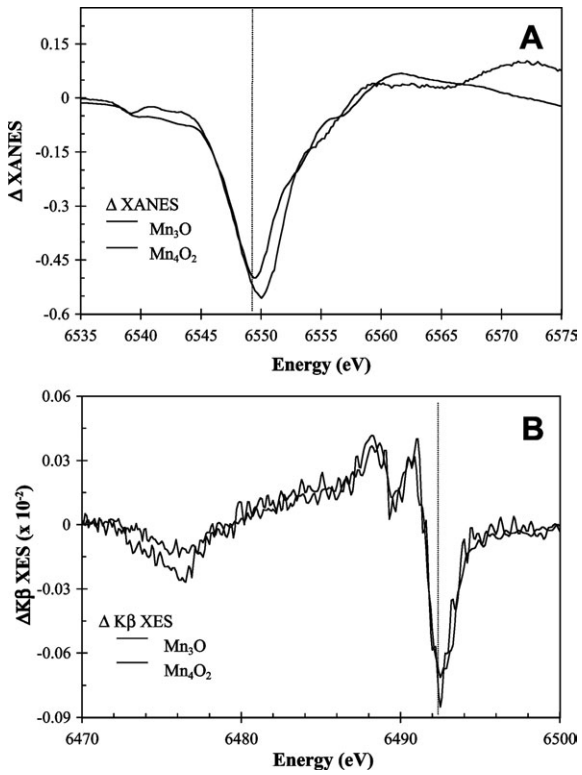

Fig. 6 Difference spectra of the (A) XANES and (B) Kβ XES profiles of the reduced minus oxidized species in each set of compounds.

3.3 Mn EXAFS

Figs. 7 and 8 show the EXAFS results of the trinuclear and tetranuclear compounds respectively. Both the *k*-space data and its Fourier transform (FT) are plotted for each compound. It is immediately obvious that the compounds containing Mn^{II} have significantly reduced *k*-space and FT amplitudes in comparison to their more oxidized counterparts. Secondly, the FT peaks are also shifted to longer apparent distances in both **Mn_3O(II)** and **Mn_4O_2(II)** to varying amounts. The decrease in FT amplitudes is caused by the presence of a distribution of Mn–Mn and Mn-ligand distances in these compounds. Hence looking at only the FT profile is misleading – the number of backscattering neighbors are not diminished, rather the *k*-space confirms that the varying Mn–X distances in these compounds result in destructive interference. For this reason, simulations of the isolated *k*-space waves are typically used for distance determination rather than inference of distances or the number of such interactions from the FTs.

Although the EXAFS simulations are not shown, we can verify from the crystallographic data[29–35] that the change in bond distances and relative angles due to Mn reduction is greater in the Mn_3O compounds, hence the much lower FT amplitudes for **Mn_3O(II)** (Fig. 7). The equilateral triangle formed by the three Mn atoms is distorted towards an isosceles configuration with a slightly shorter Mn–Mn distance between the Mn^{III} atoms. More importantly, the Mn–O distance to the central oxygen atom is much longer (2.15 Å) for the Mn^{II} atom than for the Mn^{III} atoms (1.82 Å) and this forces the central oxygen atom to a position that is slightly above the plane formed by the Mn atoms. Additionally, there is a wide range in the short distance interactions to Mn by neighboring oxygen or nitrogen ligands (1.95–2.24 Å) and this serves to decrease the observed FT and *k*-space amplitudes though destructive interference. In the Mn_4O_2 compounds the observed effect is less severe because the Mn^{II} atom occupies one of the wing positions rather than the central di-μ-oxo bridged Mn core

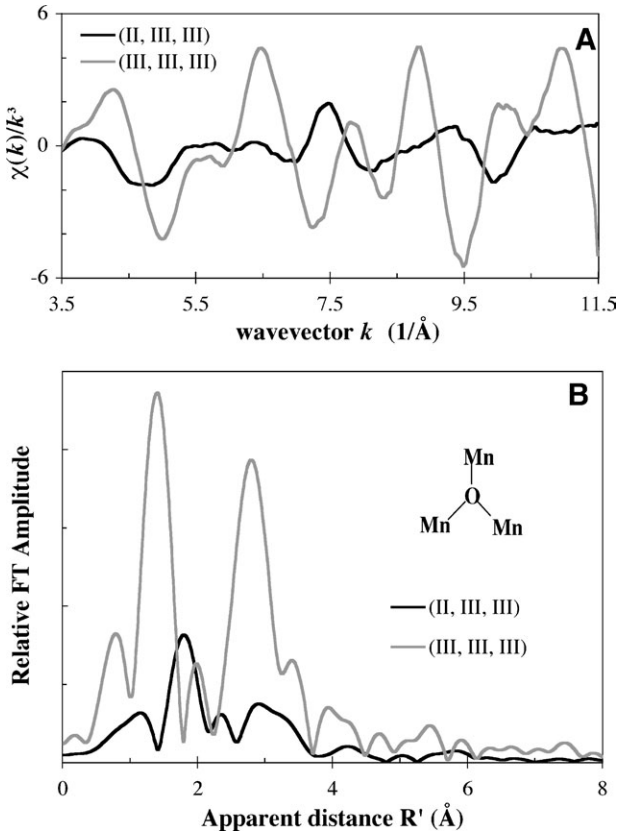

Fig. 7 Mn EXAFS (A) *k*-space (weighed by k^3) and (B) its Fourier transform for each of the **Mn_3O** compounds.

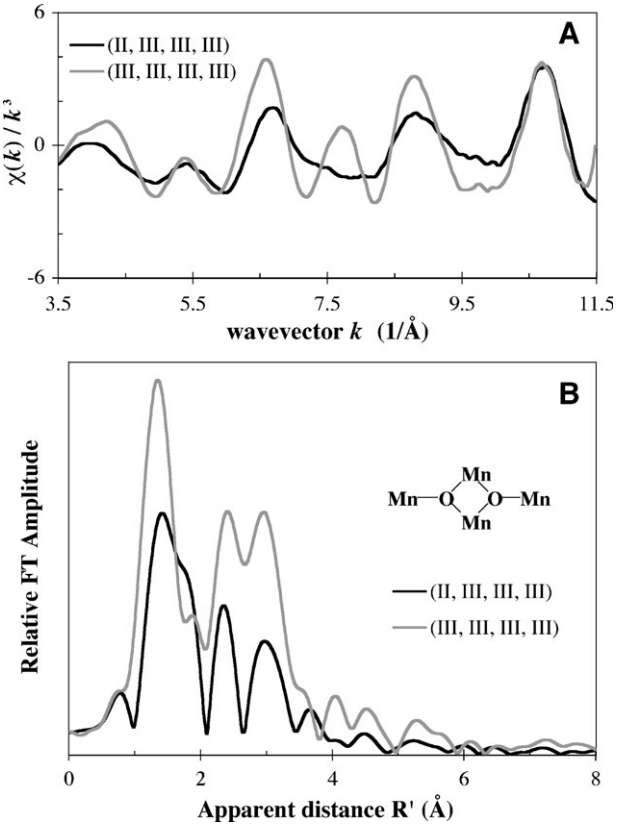

Fig. 8 Mn EXAFS (A) *k*-space (weighed by k^3) and (B) its Fourier transform for each of the **Mn_4O_2** compounds.

(Fig. 2). The Mn–Mn bond distance among the two di-μ-oxo bridged Mn atoms is comparable for both oxidized and reduced compounds (2.85 Å and 2.78 Å) while the mono-μ-oxo bridged Mn atoms are further differentiated according to the number of benzoate ligands. In **Mn_4O_2(III)**, the difference in the average Mn–Mn distance due to one *vs.* two benzoate ligands is small (3.38 Å *vs.* 3.31 Å) while in **Mn_4O_2(II)** there is a larger difference (3.39 Å *vs.* 3.54 Å) as demonstrated by the better differentiation of the FT shoulder/peak near apparent distance R′ = 3.5 Å.

4 Discussion

Motivated by the Mn cluster of the photosynthetic oxygen evolving center, this study uses Mn model compounds with homologous structures but differing oxidation states to examine the effect of Mn oxidation on the observed X-ray spectra. Previous studies of the individual S-states of the OEC show that Mn is oxidized during the $S_0 \rightarrow S_1$ and $S_1 \rightarrow S_2$ transitions, however, there is a long-standing controversy concerning the involvement of Mn oxidation in the $S_2 \rightarrow S_3$ transition. Based on XANES data, Ono *et al.*[27] and Iuzzolino *et al.*[28] conclude that Mn oxidation is involved in this transition whereas Roelofs *et al.*[36] support a ligand-centered oxidation due to the lack of a significant energy shift in the XANES spectra between S_2 and S_3. Because Kβ XES is less sensitive to ligand effects than XANES, it has been recently applied to the individual S-states of the OEC. Messinger *et al.*[26] conclude that the small energy shifts in both XANES and XES, relative to those observed for the $S_0 \rightarrow S_1$ and $S_1 \rightarrow S_2$ transitions, support a ligand-centered oxidation during the $S_2 \rightarrow S_3$ transition. Nevertheless, it has been argued that an opposing effect could cause the lack of an energy shift in XANES and Kβ XES data; namely, a structural change in the OEC during the $S_2 \rightarrow S_3$ transition which offsets the effects due to Mn oxidation. To resolve this issue, the influence of oxidation-state and structural changes on XANES and Kβ XES spectra needs to be

established. This study presents a set of trinuclear Mn complexes in oxidation states (III_3) and (II,III_2), and a set of tetranuclear complexes in oxidation states (III_4) and (II,III_3), that are characterized using XAS and Kβ XES.

The Mn XANES K-edge is sensitive to changes in oxidation state and ligand environment that are manifested as shifts in the observed inflection point energy (IPE) as well as changes in the overall band shape. Conversely Kβ XES is the result of an exchange interaction between the 3d and 3p orbitals.[39] The splitting between the Kβ′ and $K\beta_{1,3}$ peaks becomes smaller for higher oxidation states because fewer 3d valence electrons are available to interact with the 3p hole.[40] Thus, in contrast to XANES, the $K\beta_{1,3}$ XES bands shift to lower energy with higher oxidation states and are less sensitive to the ligand environment. The energy values of $K\beta_{1,3}$ bands are calculated using the first moment integration over a set energy region. Because the entire $K\beta_{1,3}$ band is included for energy determination rather than the single point IPE used in XANES, it is much less sensitive to the chosen integration limits and is well suited to reliably quantify small energy shifts.

Different in nature, XANES and XES provide complementary insights and our results show that these techniques are a powerful combination for detecting changes in oxidation state. We see that the Mn K-edge XANES spectra shift to higher energy and the XES $K\beta_{1,3}$ peak shifts to lower energy upon oxidation in each of the two sets of compounds examined (Figs. 3–5). Not surprisingly, the XANES difference spectra (Fig. 6A) for the two sets of compounds are distinct from each other especially in the region >6555 eV where ligand interactions have a higher influence. Also the shifts in IPE between the two sets of compounds are notably different (1.64 eV for Mn_3O *vs.* 2.20 eV in Mn_4O_2). Therefore, care must be exercised when correlating the Mn K-edge energies to Mn oxidation states without taking into account the nature of the ligand environment and the overall structure of the compound. For example, in the XANES of the Mn_3O compounds the intensity of the pre-edge feature increases when the center of symmetry is disrupted by the Mn^{II} or when the overall symmetry is lower (other ligands in **Mn_3O(II)**). In the Mn_4O_2 compounds, the pre-edge feature is also slightly higher for **Mn_4O_2(II)**. The effects of symmetry and bonding are evident in the EXAFS region where both **Mn_3O(II)** and **Mn_4O_2(II)** have greatly decreased *k*-space and FT amplitudes, as compared to their respective structural analogs. This is due to a broader distribution of neighboring interactions. Detailed in the Results section, the range of Mn-ligand distances and angles is wider for the reduced compounds and this leads to destructive interference in the *k*-space wave thus decreased FT profiles. This is particularly apparent in the trinuclear compounds where the short distance interactions to the Mn^{II} are noticeably longer than for the Mn^{III} atoms. The FT profile of **Mn_4O_2(II)** is not as affected as that of **Mn_3O(II)** because the Mn^{II} atom is not located at the di-μ-oxo core structure, nevertheless a decrease in amplitude and shifts to longer apparent distances are similarly observed. In short, the dramatic differences detected in the FT profiles of these compounds show that EXAFS analysis is especially sensitive to the ligand environment. With this in mind, we would like to note that previous EXAFS characterization of the Mn_4Ca cluster of the OEC at each S-state[14–17] show that the structural changes observed after each oxidizing step are comparable to those measured in these model compounds (Mn–Mn distance changes of 0.1–0.3 Å). The reported XANES K-edge energy shift for $S_0 \rightarrow S_1$ (proposed $Mn^{II \rightarrow III}$ oxidation)[16–18] is also comparable in magnitude to those observed in this study, while the K-edge energy shifts for the $S_1 \rightarrow S_2$ and $S_2 \rightarrow S_3$ transitions are smaller. Evidently both Mn oxidation and ligand interactions have an effect on the observed XAS.

In contrast to XANES and EXAFS, the Kβ XES spectra show much less dependence on ligand environment or the structure of the complex (Figs. 5 and 6B). Despite differences in the structure of Mn_3O and Mn_4O_2, the effect of the Mn oxidation change on the XES of both sets of compounds is remarkably similar. The change in the $K\beta_{1,3}$ 1st moment values is 0.12 eV in the trinuclear compounds *vs.* 0.09 eV for the tetranuclear compounds. In addition, the profiles of the difference spectra between reduced and oxidized species are very similar for the two sets (Fig. 6B). The small difference in the intensity is consistent with the fact that in the trinuclear complex, one of three Mn^{III} is being reduced, while only one out of four Mn^{III} is being reduced in the tetranuclear complex. Comparison with the larger spectral changes observed in XANES indicates that the XES technique is less sensitive to the structure or ligands of the complex and predominantly dependent on the oxidation state. This is supported by a previous XES study of Mn model compounds where Visser *et al.*[25] showed uniform 0.20 to 0.22 eV decreases in the $K\beta_{1,3}$ first moment energy for a set of electrochemically prepared Mn-oxo binuclear compounds with $Mn(II,III \rightarrow III,IV \rightarrow IV,IV)$ oxidation state changes. The deconvoluted Kβ XES difference spectra for those compounds were also remarkably similar regardless of structural differences thus demonstrating that XES is a reliable measure of oxidation state changes rather than ligand effects. In PSII,Messinger *et al.* observed a shift of 0.06 eV in the $K\beta_{1,3}$ first moment energy for the $S_1 \rightarrow S_2$ transition where 1 Mn out of 4 is oxidized, and a shift of 0.02 eV for the $S_2 \rightarrow S_3$ transition. Accompanied by subtle structural changes in the Mn_4Ca cluster detected in EXAFS, these small $K\beta_{1,3}$ shifts are nonetheless accurate measures of changes in the Mn oxidation state. Combining this technique with results from XANES and electron paramagnetic (EPR) measurements reinforce the proposal for a ligand-centered oxidation during the $S_2 \rightarrow S_3$ transition.

In conclusion, XAS studies on structurally homologous model compounds provide a meaningful reference point for interpretation of the data from PS II. The work presented here confirms that shifts in both XANES and XES should be observed upon changes in Mn oxidation, but for XES such shifts are quantitatively related to the oxidation state. Additionally, it supports Messinger *et al.*'s assignment of Mn oxidation states and changes in oxidation states in the OEC during the S-state transitions.

Acknowledgements

The authors thank Drs Johannes Messinger, Roehl M. Cinco, and Karen MacFarlane-Holman for help with XAS data collection. We are very grateful to Prof. Steve Cramer for the use of the emission spectrometer. Funding for this work was provided by the National Institutes of Health (GM-55302) and by the Director, Office of Basic Energy Sciences, Division of Energy Biosciences of the US Department of Energy under contract No. DE-AC03-76SF-00098. Synchrotron radiation facilities were provided by the Stanford Synchrotron Radiation Laboratory, a national user facility operated by Stanford University on behalf of the US Department of Energy, Office of Basic Energy Sciences. The SSRL Structural Molecular Biology Program is supported by the Department of Energy, Office of Biological and Environmental Research, and by the National Institutes of Health, National Center for Research Resources, Biomedical Technology Program.

References

1 R. G. Shulman, Y. Yafet, P. Eisenberger and W. E. Blumberg, *Proc. Natl. Acad. Sci. USA.*, 1976, **73**, 1384.
2 S. P. Cramer, T. K. Eccles, F. Kutzler, K. O. Hodgson and S. Doniach, *J. Am. Chem. Soc.*, 1976, **98**, 8059.
3 L. Powers, W. E. Blumberg, B. Chance, C. H. Barlow, J. S. Leigh, Jr., J. Smith, T. Yonetani, S. Vik and J. Peisach, *Biochim. Biophys. Acta*, 1979, **546**, 520.

4 J. A. Kirby, D. B. Goodin, T. Wydrzynski, A. S. Robertson and M. P. Klein, *J. Am. Chem. Soc*., 1981, **103**, 5537.
5 D. B. Goodin, V. K. Yachandra, R. D. Britt, K. Sauer and M. P. Klein, *Biochim. Biophys. Acta*, 1984, **767**, 209.
6 A. L. Roe, D. J. Schneider, R. J. Mayer, J. W. Pyrz, J. Widom and L. Que, *J. Am. Chem. Soc*., 1984, **106**, 1676.
7 N. J. Blackburn, F. C. Rhames, M. Ralle and S. Jaron, *J. Biol. Inorg. Chem*., 2000, **5**, 341.
8 U. Bergmann, M. M. Grush, C. R. Horne, P. DeMarois, J. E. Penner-Hahn, C. F. Yocum, D. W. Wright, C. E. Dubé, W. H. Armstrong, G. Christou, H. J. Eppley and S. P. Cramer, *J. Phys. Chem. B*, 1998, **102**, 8350.
9 U. Bergmann and S. P. Cramer, in *SPIE Conference on Crystal and Multilayer Optics*, SPIE, San Diego CA, 1998, **vol. 3448**, p. 198.
10 B. Kok, B. Forbush and M. McGloin, *Photochem. Photobiol*., 1970, **11**, 457.
11 N. Kamiya and J. R. Shen, *Proc. Natl. Acad. Sci. USA*, 2003, **100**, 98.
12 A. Zouni, H.-T. Witt, J. Kern, P. Fromme, N. Krauss, W. Saenger and P. Orth, *Nature*, 2001, **409**, 739.
13 K. N. Ferreira, T. M. Iverson, K. Maghlaoui, J. Barber and S. Iwata, *Science*, 2004, **303**, 1831.
14 V. J. DeRose, I. Mukerji, M. J. Latimer, V. K. Yachandra, K. Sauer and M. P. Klein, *J. Am. Chem. Soc*., 1994, **116**, 5239.
15 R. M. Cinco, A. Rompel, H. Visser, G. Aromi, G. Christou, K. Sauer, M. P. Klein and V. K. Yachandra, *Inorg. Chem*., 1999 **38**, 5988.
16 J. H. Robblee, R. M. Cinco and V. K. Yachandra, *Biochim. Biophys. Acta*, 2001, **1503**, 7.
17 V. K. Yachandra, *Philos. Trans. R. Soc. London Ser. B*, 2002 **357**, 1347.
18 J. E. Penner-Hahn, R. M. Fronko, V. L. Pecoraro, C. F. Yocum, S. D. Betts and N. R. Bowlby, *J. Am. Chem. Soc*., 1990, **112**, 2549.
19 R. M. Cinco, C. Fernandez, J. Messinger, J. H. Robblee, H. Visser, K. L. McFarlane, U. Bergmann, P. Glatzel, S. P. Cramer, K. Sauer, V. K. Yachandra and M. P. Klein in *Photosynthesis: Mechanisms and Effects*, ed. G. Garab, Kluwer Academic Publishers, Dordrecht, 1998, **vol. 2**, p.1273.
20 R. M. Cinco, K. L. M. Holman, J. H. Robblee, J. Yano, S. A. Pizzarro, E. Bellacchio, K. Sauer and V. K. Yachandra, *Biochemistry*, 2002, **41**, 12928.
21 F. DeGroot, *Chem. Rev*., 2001, **101**, 1779.
22 K. Tsutsumi, H. Nakamori and K. Ichikawa, *Phys. Rev. B*, 1976, **13**, 929.
23 P. Glatzel, U. Bergmann, F. M. F. de Groot and S. P. Cramer, *Phys. Rev. B*, 2001, **64**, 45109.
24 U. Bergmann, P. Glatzel, J. H. Robblee, J. Messinger, C. Fernandez, R. Cinco, H. Visser, K. McFarlane and E. Bellacchio *et al*., *J. Synchrotron Radiat*., 2001, **8**, 199.
25 H. Visser, E. Anxolabéhère-Mallart, U. Bergmann, P. Glatzel, J. H. Robblee, S. P. Cramer, J.-J. Girerd, K. Sauer, M. P. Kelvin and V. K. Yachandra, *J. Am. Chem. Soc*., 2001, **123**, 7031.
26 J. Messinger, J. H. Robblee, U. Bergmann, C. Fernandez, P. Glatzel, H. Visser, R. M. Cinco, K. L. McFarlane, E. Bellacchio, S. A. Pizarro, S. P. Cramer, K. Sauer, M. P. Klein and V. K. Yachandra, *J. Am. Chem. Soc*., 2001, **123**, 7804.
27 T. Ono, T. Noguchi, Y. Inoue, M. Kusunoki, T. Matsushita and H. Oyanagi, *Science*, 1992, **258**, 1335.
28 L. Iuzzolino, J. Dittmer, W. Dörner, W. Meyer-Klaucke and H. Dau, *Biochemistry*, 1998, **37**, 17112.
29 H. J. Eppley, N. deVries, S. Y. Wang, S. M. Aubin, H.-L. Tsai, K. Folting, D. N. Hendrickson and G. Christou, *Inorg. Chim. Acta*, 1997, **263**, 323.
30 J. B. Vincent, H. R. Chang, K. Folting, J. C. Huffman, G. Christou and D. N. Hendrickson, *J. Am. Chem. Soc*., 1987, **109**, 5703.
31 J. Ribas, B. Albela, H. Stoeckli-Evans and G. Christou, *Inorg. Chem*., 1997, **36**, 2352.
32 J. B. Vincent, C. Christmas, H. R. Chang, Q. Li, P. D. W. Boyd, J. C. Huffman, D. N. Hendrickson and G. Christou, *J. Am. Chem. Soc*., 1989, **111**, 2086.
33 J. B. Vincent, C. Christmas, J. C. Huffman, G. Christou, H. R. Chang and D. N. Hendrickson, *J. Chem. Soc. Chem. Commun*., 1987, 236.
34 M. W. Wemple, H.-L. Tsai, S. Wang, J. P. Claude, W. E. Streib, J. C. Huffman, D. N. Hendrickson and G. Christou, *Inorg. Chem*., 1996, **35**, 6437.
35 B. Albela, G. Chottard and J.-J. Girerd, *J. Biol. Inorg. Chem*., 2001, **6**, 430.
36 T. A. Roelofs, M. C. Liang, M. J. Latimer, R. M. Cinco, A. Rompel, J. C. Andrews, K. Sauer, V. K. Yachandra and M. P. Klein, *Proc. Natl. Acad. Sci. USA*, 1996, **93**, 3335.
37 J. Jaklevic, J. A. Kirby, M. P. Klein, A. S. Robertson, G. S. Brown and P. Eisenberger, *Solid State Commun*., 1997, **23**, 679.
38 M. J. Latimer, V. J. DeRose, I. Mukerji, V. K. Yachandra, K. Sauer and M. P. Klein, *Biochemistry*, 1995, **34**, 10898.
39 G. Peng, F. M. F. de Groot, K. Hämäläinen, J. A. Moore, X. Wang, M. M. Grush, J. B. Hastings, D. P. Siddons and W. H. Armstrong *et al*., *J. Am. Chem. Soc*., 1994, **116**, 2914.
40 M. Taguchi, T. Uozumi and A. Kotani, *J. Phys. Soc. Jpn*., 1997, **66**, 247.

